Quantitative Atomic Resolution Force Imaging on Epitaxial Graphene with Reactive and Nonreactive AFM Probes

Mark P. Boneschanscher,[†] Joost van der Lit,[†] Zhixiang Sun,[†,‡] Ingmar Swart,[†] Peter Liljeroth,[§,*] and Daniël Vanmaekelbergh[†,*]

[†]Condensed Matter and Interfaces, Debye Institute for Nanomaterials Science, Utrecht University, P.O. Box 80000, 3508 TA Utrecht, The Netherlands, [‡]Max Planck Institute for Solid State Research, Heisenbergstrasse 1, 70569 Stuttgart, Germany, and [§]Department of Applied Physics, Aalto University School of Science, P.O. Box 15100, 00076 Aalto, Finland

ABSTRACT Atomic force microscopy (AFM) images of graphene and graphite show contrast with atomic periodicity. However, the contrast patterns vary depending on the atomic termination of the AFM tip apex and the tip–sample distance, hampering the identification of the atomic positions. Here, we report quantitative AFM imaging of epitaxial graphene using inert (carbon-monoxide-terminated) and reactive (iridium-terminated) tips. The atomic image contrast is markedly different with these tip terminations. With a reactive tip, we observe an inversion from attractive to repulsive atomic contrast with decreasing tip–sample distance, while a nonreactive tip only yields repulsive atomic contrast. We are able to identify the atoms with both tips at any tip–sample distance. This is a prerequisite for future structural and chemical analysis of adatoms, defects, and the edges of graphene nanostructures, crucial for understanding nanoscale graphene devices.

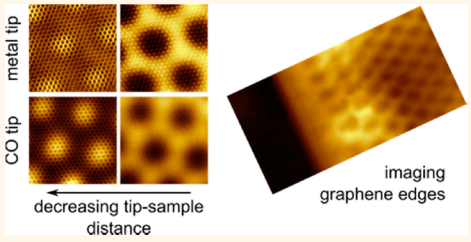

KEYWORDS: atomic force microscopy · AFM · graphene · Ir(111) atomic contrast · graphene edge

The relationship between the atomic configuration and electronic structure in graphene nanostructures has attracted tremendous interest.[1–4] While scanning tunneling microscopy (STM) has proven extremely useful in acquiring local electronic information,[5–8] the study of the atomic structure with STM is complicated: the contrast in the tunneling current is more sensitive to the electronic structure close to the Fermi level than to the atomic geometry.[9–11] In frequency modulation AFM (FM-AFM), the frequency shift Δf of the oscillating tip due to the tip–sample interaction is measured.[12] Sub-angstrom tip oscillation amplitudes enhance the sensitivity to short-range forces, leading to improved spatial resolution.[13–15] The image resolution can further be improved by controlled modification of the chemical reactivity of the AFM tip apex by picking up adatoms or small inorganic molecules.[14,16–18] AFM images of graphene and graphite show contrast with atomic periodicity.[19–21] However, the contrast patterns vary depending on the atomic termination of the AFM tip apex and the tip–sample distance, hampering the identification of the atomic positions.[22–24]

Previous AFM experiments on carbon nanotubes and graphite showed a maximum attractive force between tip and sample on lattice sites with a triangular periodicity, consistent with either the hollow sites or every other atom of the carbon lattice.[21,25,26] Using a Lennard-Jones model, this attraction was explained to originate from the hollow site.[27] It was only with the advent of AFM imaging with very low tip oscillation amplitudes that image contrast with a honeycomb lattice was achieved on graphite.[20,23,28] Simultaneous AFM and STM were used to measure both force and current landscapes above graphite and epitaxial graphene.[19,22] The topographies were found to differ strongly depending on bias settings and distance, making identification of the true positions of the carbon atoms difficult.

The role of tip termination and reactivity in imaging graphene has not been experimentally studied. A recent theoretical paper based on density functional theory (DFT) calculations indicated that account of the tip reactivity should be a key for understanding the wide variety in measured topographies.[24] The model predicts that, for nonreactive tips, atomic scale contrast will only be observed in the repulsive regime. For reactive tips, an as-yet unobserved inversion of the atomic contrast

* Address correspondence to peter.liljeroth@aalto.fi, d.vanmaekelbergh@uu.nl.

Received for review August 31, 2012 and accepted October 6, 2012.

Published online October 07, 2012
10.1021/nn3040155

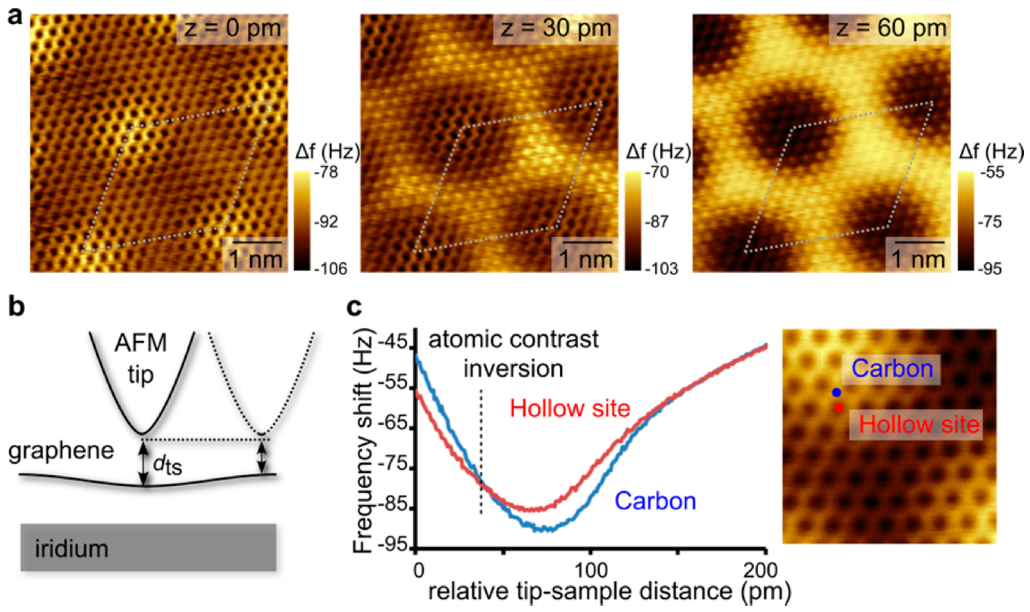

Figure 1. Constant height AFM imaging of epitaxial graphene on Ir(111) with a metallic tip. (a) Constant height Δf images acquired with a metallic iridium tip at varying d_{ts}. All scans are 5 × 5 nm^2, and the relative tip heights are indicated in the insets. The moiré unit cell is indicated by the dotted lines. Regions with brighter contrast correspond to less negative Δf (smaller attractive force). (b) Schematic of the variation of the tip−sample distance going from the middle to the corner of the moiré unit cell. (c) Frequency shift *vs* tip−sample distance measured above the position of a carbon atom (blue curve) and a hollow site (red curve). The distance where the atomic scale contrast inverts is indicated by a dashed vertical line. The inset acquired in the repulsive regime shows the positions of the Δf *vs* d_{ts} curves.

upon variation of the tip−sample distance (d_{ts}) is anticipated. This inversion results from a change in interaction between tip and carbon atoms from maximum attraction at sufficiently large d_{ts} into a minimum attractive force when Pauli repulsion becomes important (at small d_{ts}).

Here, we present a study of the effect of tip reactivity in imaging the atoms of epitaxial graphene using a nonreactive, carbon monoxide (CO)-terminated tip and a reactive Ir tip. We examine the image contrast with both tips at various d_{ts}, ranging from the attractive regime to the onset of the Pauli repulsion regime. This allows us to provide a consistent interpretation of the atomic scale contrast patterns at any tip−sample distance and to identify the carbon atoms in the lattice and edges of graphene.

RESULTS AND DISCUSSION

Figure 1 shows a series of Δf images acquired at constant height using an iridium-terminated tip. A reference distance of d_{ts} = 0 is chosen for the closest tip−sample distance that could be achieved while keeping the tip stable. The patterns reflect the periodicity of carbon atoms in graphene and on a larger length scale (*ca.* 2.5 nm) a periodicity consistent with the moiré unit cell for graphene on Ir(111).[29] The moiré pattern is set up by the lattice mismatch between graphene and the Ir(111) substrate, resulting in a topographic corrugation of the graphene layer, as illustrated in Figure 1b.[19,30] For the metallic tip, atomic contrast can already be observed in the attractive regime. A triangular pattern of light yellow dots (smaller attraction) and dark spots (stronger attraction) is observed. Previously, such patterns were measured on carbon nanotubes and graphite; the sites corresponding to maximum attraction were interpreted as corresponding to the hollow sites.[21,23,25] Here, we present an interpretation that is in contrast with this: the positions of maximum attraction (dark points) correspond to the carbon atoms in the graphene lattice, while the spots of weaker attraction (light spots) correspond to the hollow sites. This interpretation will be corroborated by the results below. A more detailed comparison including simultaneously measured tunneling current can be found in the Supporting Information. At the smallest distance, the contrast pattern is drastically changed into a lighter honeycomb lattice (smaller attraction) with in between dark dots (stronger attraction). The honeycomb lattice corresponds to the atomic backbone of the graphene. Hence, the positions with smallest attractive force (light) represent the carbon atoms. That the left and right images represent a true contrast inversion is proven by the frequency shift−distance curves: position 1 on the light honeycomb lattice and position 2 on top of a dark spot. The Δf *versus* d_{ts} curves (Figure 1c) acquired on these two positions show a crossing and hence reflect the inversion of the contrast pattern with distance. Similar curves are obtained at different regions of the moiré pattern (Supporting Information). We remark that this contrast inversion was predicted by DFT calculations.[24] The AFM image acquired at intermediate height

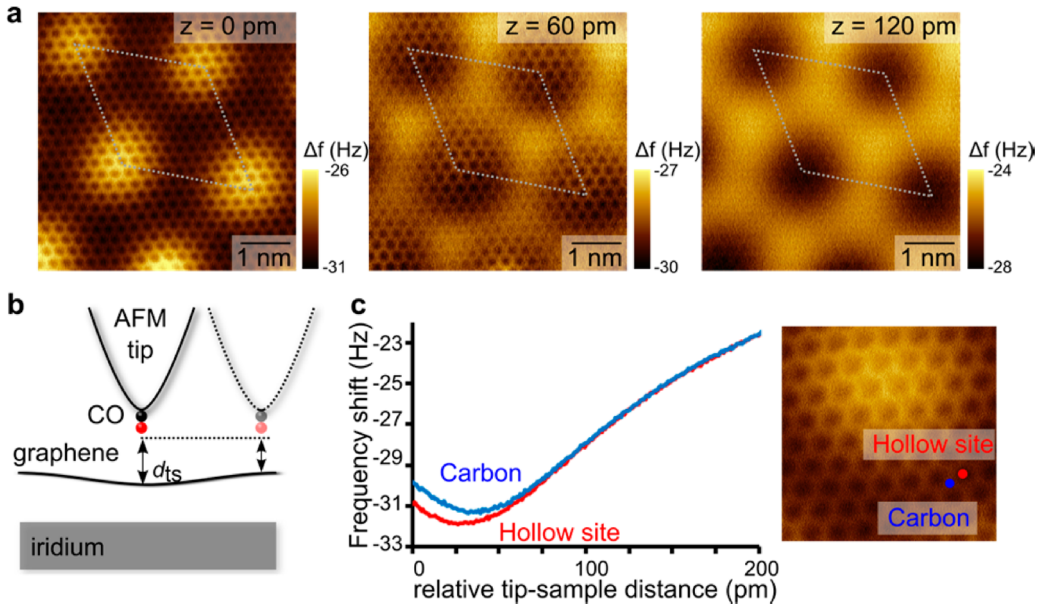

Figure 2. Constant height experiments with a CO-terminated tip. (a) Constant height Δf images acquired with a CO-terminated tip at varying d_{ts}. All scans are 5 × 5 nm^2, and the relative tip heights are indicated in the insets. The moiré unit cell is indicated by the dotted lines. Regions with brighter contrast correspond to less negative Δf (smaller attractive force). (b) Schematic of the CO-terminated tip scanning in constant height over the moiré unit cell. (c) Frequency shift *vs* tip−sample distance measured above the position of a carbon atom (blue curve) and a hollow site (red curve). The inset acquired in the repulsive regime shows the positions of the Δf *vs* d_{ts} curves.

(Figure 1a, center) shows the honeycomb lattice on the atop regions in the corners of the moiré unit cell (typical for short distances, similar to the left picture), while in the lower parts, the contrast pattern typically acquired at larger distances (similar to the right picture) is still visible.

With nonreactive CO-terminated tips, the contrast patterns are remarkably different. At large d_{ts} (Figure 2a, right), only the atop positions of the moiré unit cell are visible. Here d_{ts} is lowered locally due to the outward buckling of the graphene, resulting in additional van der Waals attraction (more negative Δf, dark, see also Figure 2b). When d_{ts} is lowered, repulsive interaction on sites forming a honeycomb lattice appears. At medium d_{ts}, this honeycomb lattice is only observed on atop positions in the moiré unit cell (Figure 2a, middle). At even lower d_{ts}, the Pauli repulsion contributes significantly to the total force and the honeycomb lattice is observed over the entire moiré unit cell (Figure 2a, left). The honeycomb lattice can be interpreted as the carbon atoms of the graphene (*i.e.*, the electronic backbone) similar to what was observed on small organic molecules.[14] Figure 2c shows the Δf *versus* d_{ts} curves acquired with the CO-terminated tip on the carbon and hollow sites, located on a lower region of the moiré pattern. Similar results are obtained at atop regions of the moiré pattern (Supporting Information).

Figures 1 and 2 demonstrate how the chemical reactivity of the tip apex controls the atomic scale contrast. As illustrated in Figure 3, the atomic scale contrast can be quantified as a function of d_{ts} by subtracting the Δf *versus* d_{ts} curve measured on top of a hollow site from the Δf *versus* d_{ts} curve measured on top of a carbon atom (examples of force curves directly calculated from the individual Δf *vs* d_{ts} curves are shown in the Supporting Information). This corrects for the overall background van der Waals interaction between tip and sample, giving us a measure for the force between the outermost tip atom (or CO molecule) and the carbon atoms in the graphene lattice. With the reactive iridium tip, we observe attractive atomic contrast in a 100 pm range of tip−sample distances. This chemical interaction between the last tip atom and the carbon atoms of the graphene results in atomic contrast (attractive or repulsive) in a d_{ts} region as broad as 150 pm. We observe a maximum attractive force on top of the carbon atom of *ca.* 150 pN (Figure 3b). This is in line with DFT calculations showing free iridium atoms adsorbing preferentially on top of the carbon atoms, not on the hollow sites.[32,33]

When d_{ts} is further reduced, we enter the regime in which Pauli repulsion becomes important. As the repulsion on carbon atoms is considerably stronger than on the hollow sites, this results in less overall attractive force (less negative Δf) on the carbon atoms. The difference in repulsion between the carbon atoms and hollow sites overcompensates the differences in the attractive forces leading to images with a honeycomb lattice. This can also be observed in the crossing of the Δf *versus* d_{ts} curves (Figure 1c) and is the reason for the change of sign in the Δf difference curve (Figure 3a).

With the chemically passivated CO-terminated tip, chemical bond formation between the tip and

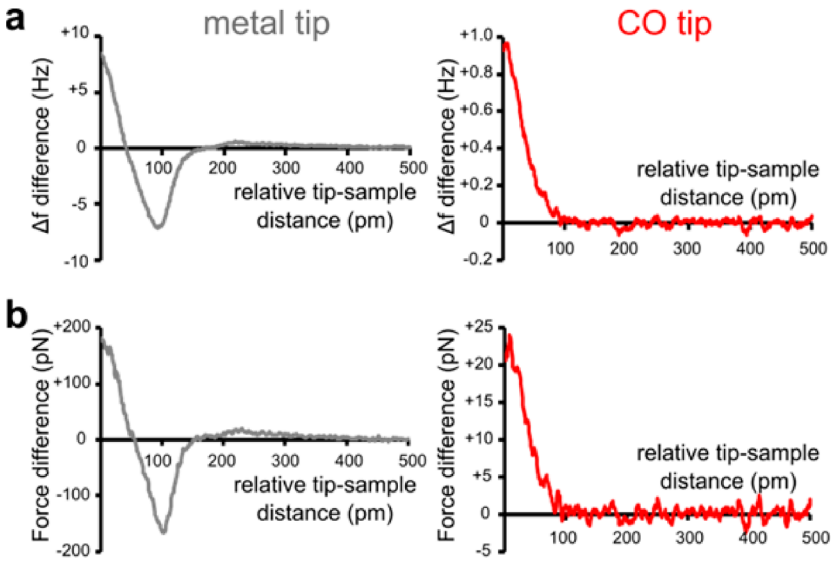

Figure 3. Force curves showing the formation of atomic scale contrast. (a) Frequency shift difference between carbon and hollow site as a function of tip–sample distance. Measured with a metal tip (gray curve) and with a CO-terminated tip (red curve). (b) Force curves calculated from the frequency shift difference curves in (a) using the Sader–Jarvis method.[31]

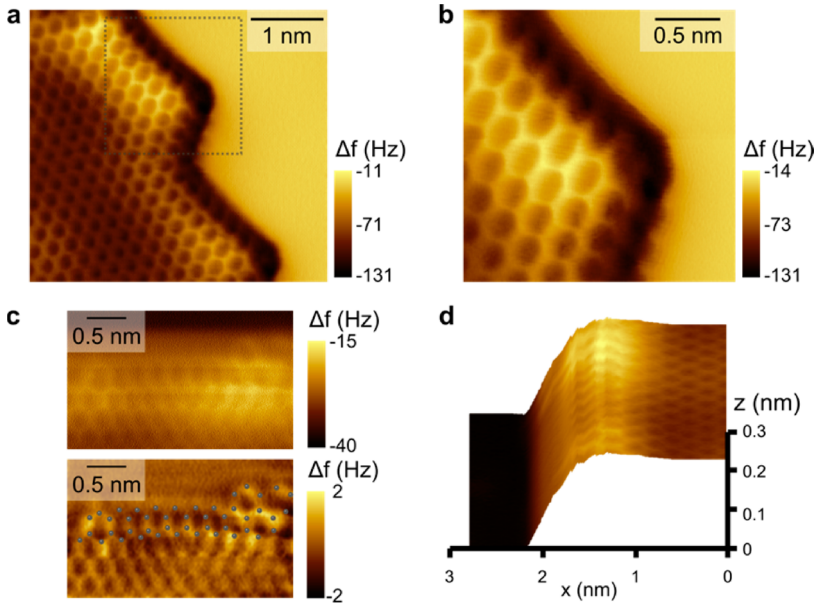

Figure 4. Frequency shift mapping of a graphene edge. (a) Constant height image of the frequency shift over a graphene edge measured with an iridium-terminated tip. (b) Zoom-in on the indicated region in (a). (c) Adaptive height scan of the frequency shift over the edge of a graphene island measured with a CO-terminated tip. Top image is raw data, bottom image after median line correction and filtering, with an overlaid schematic indicating the positions of the outermost benzene rings. (d) Filtered image from (c) mapped to the height profile that the tip followed while scanning over the edge. The height profile is determined prior to scanning using STM feedback (100 mV, 30 pA).

graphene does not occur (Figure 3a). The difference in van der Waals attraction for the carbon atoms and hollow sites is too small to be visible as an atomic scale contrast in the image. Atomic contrast is only observed at smaller d_{ts}, in the Pauli repulsion regime. We find a maximum repulsive force on top of the carbon atoms of *ca.* 25 pN. This is in good agreement with the observed repulsive force contrast of *ca.* 10 pN with a CO-modified tip on a pentacene molecule.[14]

Understanding the contrast formation on graphene enables us to analyze the edge structure of graphene nanostructures, which is one of the key challenges in realizing graphene-based nanoelectronics. In Figure 4, we show first results of graphene islands on Ir(111). The islands are terminated along the zigzag direction, but STM experiments have been unable to detect the theoretically predicted edge states. One possible reason for this is bonding between the graphene edge and the underlying iridium substrate.

Due to the changing slope of the Δf *versus* d_{ts} curve and strong changes in the tip–sample interaction, it is impossible to image the graphene edges in the Pauli repulsion regime using Δf feedback. We found that, for the metal tip, the best results were obtained using constant height scans over the graphene edge in the Pauli repulsion regime (Figure 4 and Supporting Information). However, the strong bending of the graphene layer toward the Ir surface at the edge makes it very hard to determine the exact atomic geometry of the outermost row of carbon atoms.

A possible solution for this problem is to use adaptive height scans with a CO-terminated tip as described in the Supporting Information. Since the CO-terminated tip is chemically inert, the tip can be brought closer to the Ir(111) substrate while scanning over the edge. This finally allows imaging of the outermost row of carbon atoms, as shown in Figure 4c. We are also able to atomically resolve one of the kinks (right side of the image), revealing that the kinks are in fact due to the onset of an additional row of benzene rings to the graphene. The distorted benzene rings and apparent changes in the carbon–carbon bond lengths close to the edge of the graphene are likely to result from the flexibility of the CO on the tip apex.[18,34] The graphene island is terminated by nonreconstructed zigzag edges that bend down by *ca.* 0.4 Å due to the increased interaction with the underlying Ir(111) substrate.

CONCLUSIONS

In conclusion, we have studied how the AFM atomic contrast in graphene depends on tip termination and tip–sample distance. This allows us to identify the atoms from any contrast pattern as demonstrated by atomic resolution imaging of graphene edges. Combined STM and AFM measurements can now be used to unravel the effect of defects, distortions, and edges on the electrical properties of graphene nanostructures.

METHODS

Graphene Growth. We grew epitaxial graphene on Ir(111) from ethylene using the temperature-programmed growth method.[35] The Ir(111) surface was cleaned by repetitive cycles of argon sputtering and flash heating to 1500 K. After the sample had cooled below 570 K, ethylene was deposited on the surface (3×10^{-6} mbar for 10 s). The temperature was then raised to 1200 K for 20 s to grow large, mostly defect-free graphene islands.

STM/AFM Experiments. After the growth, the sample was inserted into a low-temperature STM/AFM ($T = 4.8$ K, Omicron LT-STM/QPlus AFM), housed within the same ultrahigh vacuum system (base pressure $<10^{-10}$ mbar). We used commercially available W tips mounted on a Qplus sensor (Omicron) with a resonance frequency f_0 of *ca.* 24.5 kHz, a quality factor of 12 000, and a peak-to-peak oscillation amplitude of 171 pm.

Constant Height Experiments. Series of constant height maps of the frequency shift Δf were recorded at different heights above the same area of graphene. Software built-in options (Matrix 3.0) were used to correct for sample tilt and tip drift. To facilitate minimum drift, the tip was kept in tunneling contact with the sample for several hours prior to the constant height scans and Δf *versus* d_{ts} spectra. Recorded topographies were averaged over trace and retrace. Although the absolute distance between tip and sample is not known, the distance between the different constant height scans can accurately be determined by measurement of Δf *versus* d_{ts} at specific sites in the image and comparing this to the recorded Δf at this site in the constant height scans. A reference distance of $d_{ts} = 0$ is chosen for the closest tip–sample distance that could be achieved while keeping the tip stable. Frequency shift as a function of the tip–sample distance (Δf *vs* d_{ts}) curves were converted to force–distance curves using the Sader–Jarvis method.[31]

Adaptive Height Experiments. Adaptive height scans were performed using height profiles obtained in STM feedback mode as input for the tip height while scanning without feedback in the Pauli repulsion regime. However, the bond formation between the metal tip and the iridium substrate induces tip changes at small d_{ts}. This can be circumvented by the use of a CO-terminated tip, which allows stable imaging over the graphene edge.

Tip Preparation. The metal tip apex was formed by controlled contact with the iridium surface, resulting in an iridium-coated metal tip. The metallic nature of the tip was confirmed by conductance spectroscopy on the iridium surface. We did not succeed in controlled pickup of a CO molecule from the Ir(111) substrate onto the tip apex. Consequently, for the experiments with CO-terminated tips, we followed the previously introduced procedure.[14,19] The tip was prepared on a Cu(111) surface, resulting in a copper-coated metal tip. Then 10^{-9} mbar of CO was leaked in the vacuum chamber for 10 s, resulting in ~1/10 monolayer of CO molecules on the copper surface. A single CO molecule was picked up as described previously; the nature of the tip apex was confirmed by the observed contrast inversion in STM feedback of the imaged CO on the copper surface. Subsequently, the Cu(111) was exchanged for the graphene-coated Ir(111) sample, after which the CO tip was carefully approached. The stability of the CO molecule on the tip apex through the experiments on the graphene was confirmed by changing back to the Cu(111) substrate with adsorbed CO molecules and checking the contrast above the CO on the copper in STM feedback.

Conflict of Interest: The authors declare no competing financial interest.

Acknowledgment. This research was supported by the Academy of Finland (the Centre of Excellence Programme No. 250280), NWO (Chemical Sciences, Vidi-grant 700.56.423, and Veni-grant 722.011.007), the European Research Council (ERC-2011-StG 278698-PRECISE-NANO) and FOM ["Control over Functional Nanoparticle Solids (FNPS)"].

Supporting Information Available: Comparison between measured frequency shifts and tunneling currents, force–distance curves measured on different sites within the moiré unit cell, and additional results on imaging graphene edges with metallic and CO-terminated tips. This material is available free of charge *via* the Internet at http://pubs.acs.org.

REFERENCES AND NOTES

1. Geim, A. K.; Novoselov, K. S. The Rise of Graphene. *Nat. Mater.* **2007**, *6*, 183–191.
2. Castro Neto, A. H.; Guinea, F.; Peres, N. M. R.; Novoselov, K. S.; Geim, A. K. The Electronic Properties of Graphene. *Rev. Mod. Phys.* **2009**, *81*, 109–162.
3. Suenaga, K.; Koshino, M. Atom-by-Atom Spectroscopy at Graphene Edge. *Nature* **2010**, *468*, 1088–1090.
4. Levy, N.; Burke, S. A.; Meaker, K. L.; Panlasigui, M.; Zettl, A.; Guinea, F.; Neto, A. H. C.; Crommie, M. F. Strain-Induced

Pseudo-Magnetic Fields Greater than 300 T in Graphene Nanobubbles. *Science* **2010**, *329*, 544–547.
5. Hämäläinen, S. K.; Sun, Z.; Boneschanscher, M. P.; Uppstu, A.; Ijäs, M.; Harju, A.; Vanmaekelbergh, D.; Liljeroth, P. Quantum-Confined Electronic States in Atomically Well-Defined Graphene Nanostructures. *Phys. Rev. Lett.* **2011**, *107*, 236803.
6. Xue, J.; Sanchez-Yamagishi, J.; Bulmash, D.; Jacquod, P.; Deshpande, A.; Watanabe, K.; Taniguchi, T.; Jarillo-Herrero, P.; LeRoy, B. J. Scanning Tunnelling Microscopy and Spectroscopy of Ultra-Flat Graphene on Hexagonal Boron Nitride. *Nat. Mater.* **2011**, *10*, 282–285.
7. Decker, R.; Wang, Y.; Brar, V. W.; Regan, W.; Tsai, H.-Z.; Wu, Q.; Gannett, W.; Zettl, A.; Crommie, M. F. Local Electronic Properties of Graphene on a Bn Substrate *via* Scanning Tunneling Microscopy. *Nano Lett.* **2011**, *11*, 2291–2295.
8. Zhao, L.; He, R.; Rim, K. T.; Schiros, T.; Kim, K. S.; Zhou, H.; Gutiérrez, C.; Chockalingam, S. P.; Arguello, C. J.; Pálová, L.; *et al.* Visualizing Individual Nitrogen Dopants in Monolayer Graphene. *Science* **2011**, *333*, 999–1003.
9. Chen, C. J. *Introduction to Scanning Tunneling Microscopy*, 2nd ed.; Oxford University Press: Oxford, UK, 2008.
10. Hofer, W. A.; Foster, A. S.; Shluger, A. L. Theories of Scanning Probe Microscopes at the Atomic Scale. *Rev. Mod. Phys.* **2003**, *75*, 1287–1331.
11. Ugeda, M.; Fernández-Torre, D.; Brihuega, I.; Pou, P.; Martínez-Galera, A.; Pérez, R.; Gómez-Rodríguez, J. Point Defects on Graphene on Metals. *Phys. Rev. Lett.* **2011**, *107*, 116803.
12. Morita, S.; Giessibl, F. J.; Wiesendanger, R. *Noncontact Atomic Force Microscopy*; Springer: Berlin, 2009; Vol. 2.
13. Giessibl, F. J. Advances in Atomic Force Microscopy. *Rev. Mod. Phys.* **2003**, *75*, 949–983.
14. Gross, L.; Mohn, F.; Moll, N.; Liljeroth, P.; Meyer, G. The Chemical Structure of a Molecule Resolved by Atomic Force Microscopy. *Science* **2009**, *325*, 1110–1114.
15. Welker, J.; Giessibl, F. J. Revealing the Angular Symmetry of Chemical Bonds by Atomic Force Microscopy. *Science* **2012**, *336*, 444–449.
16. Gross, L.; Mohn, F.; Moll, N.; Meyer, G.; Ebel, R.; Abdel-Mageed, W. M.; Jaspars, M. Organic Structure Determination Using Atomic-Resolution Scanning Probe Microscopy. *Nat. Chem.* **2010**, *2*, 821–825.
17. Moll, N.; Gross, L.; Mohn, F.; Curioni, A.; Meyer, G. The Mechanisms Underlying the Enhanced Resolution of Atomic Force Microscopy with Functionalized Tips. *New J. Phys.* **2010**, *12*, 125020.
18. Sun, Z.; Boneschanscher, M. P.; Swart, I.; Vanmaekelbergh, D.; Liljeroth, P. Quantitative Atomic Force Microscopy with Carbon Monoxide Terminated Tips. *Phys. Rev. Lett.* **2011**, *106*, 046104.
19. Sun, Z.; Hämäläinen, S. K.; Sainio, J.; Lahtinen, J.; Vanmaekelbergh, D.; Liljeroth, P. Topographic and Electronic Contrast of the Graphene Moire on Ir(111) Probed by Scanning Tunneling Microscopy and Noncontact Atomic Force Microscopy. *Phys. Rev. B* **2011**, *83*, 081415.
20. Hembacher, S.; Giessibl, F. J.; Mannhart, J.; Quate, C. F. Revealing the Hidden Atom in Graphite by Low-Temperature Atomic Force Microscopy. *Proc. Natl. Acad. Sci. U.S.A.* **2003**, *100*, 12539–12542.
21. Hölscher, H.; Allers, W.; Schwarz, U. D.; Schwarz, A.; Wiesendanger, R. Interpretation of "True Atomic Resolution" Images of Graphite (0001) in Noncontact Atomic Force Microscopy. *Phys. Rev. B* **2000**, *62*, 6967–6970.
22. Hembacher, S.; Giessibl, F. J.; Mannhart, J.; Quate, C. F. Local Spectroscopy and Atomic Imaging of Tunneling Current, Forces, and Dissipation on Graphite. *Phys. Rev. Lett.* **2005**, *94*, 056101.
23. Albers, B. J.; Schwendemann, T. C.; Baykara, M. Z.; Pilet, N.; Liebmann, M.; Altman, E. I.; Schwarz, U. D. Three-Dimensional Imaging of Short-Range Chemical Forces with Picometre Resolution. *Nat. Nanotechnol.* **2009**, *4*, 307–310.
24. Ondráček, M.; Pou, P.; Rozsíval, V.; González, C.; Jelínek, P.; Pérez, R. Forces and Currents in Carbon Nanostructures: Are We Imaging Atoms? *Phys. Rev. Lett.* **2011**, *106*, 176101.
25. Ashino, M.; Schwarz, A.; Behnke, T.; Wiesendanger, R. Atomic-Resolution Dynamic Force Microscopy and Spectroscopy of a Single-Walled Carbon Nanotube: Characterization of Interatomic van der Waals Forces. *Phys. Rev. Lett.* **2004**, *93*, 136101.
26. Allers, W.; Schwarz, A.; Schwarz, U. D.; Wiesendanger, R. Dynamic Scanning Force Microscopy at Low Temperatures on a van der Waals Surface: Graphite (0001). *Appl. Surf. Sci.* **1999**, *140*, 247–252.
27. Hölscher, H.; Allers, W.; Schwarz, U. D.; Schwarz, A.; Wiesendanger, R. Determination of Tip−Sample Interaction Potentials by Dynamic Force Spectroscopy. *Phys. Rev. Lett.* **1999**, *83*, 4780–4783.
28. Kawai, S.; Kawakatsu, H. Surface-Relaxation-Induced Giant Corrugation on Graphite (0001). *Phys. Rev. B* **2009**, *79*, 115440.
29. N'Diaye, A. T.; Coraux, J.; Plasa, T. N.; Busse, C.; Michely, T. Structure of Epitaxial Graphene on Ir(111). *New J. Phys.* **2008**, *10*, 043033.
30. Busse, C.; Lazić, P.; Djemour, R.; Coraux, J.; Gerber, T.; Atodiresei, N.; Caciuc, V.; Brako, R.; N'Diaye, A. T.; Blügel, S.; *et al.* Graphene on Ir(111): Physisorption with Chemical Modulation. *Phys. Rev. Lett.* **2011**, *107*, 036101.
31. Sader, J. E.; Jarvis, S. P. Accurate Formulas for Interaction Force and Energy in Frequency Modulation Force Spectroscopy. *Appl. Phys. Lett.* **2004**, *84*, 1801–1803.
32. Feibelman, P. J. Pinning of Graphene to Ir(111) by Flat Ir Dots. *Phys. Rev. B* **2008**, *77*, 165419.
33. Feibelman, P. J. Onset of Three-Dimensional Ir Islands on a Graphene/Ir(111) Template. *Phys. Rev. B* **2009**, *80*, 085412.
34. Gross, L.; Mohn, F.; Moll, N.; Schuler, B.; Criado, A.; Guitián, E.; Peña, D.; Gourdon, A.; Meyer, G. Bond-Order Discrimination by Atomic Force Microscopy. *Science* **2012**, *337*, 1326–1329.
35. Coraux, J.; N'Diaye, A. T.; Engler, M.; Busse, C.; Wall, D.; Buckanie, N.; Meyer zu Heringdorf, F.-J.; van Gastel, R.; Poelsema, B.; Michely, T. Growth of Graphene on Ir(111). *New J. Phys.* **2009**, *11*, 023006.